IEEE Access
Multidisciplinary | Rapid Review | Open Access Journal

Received March 25, 2022, accepted April 13, 2022, date of publication April 20, 2022, date of current version May 16, 2022.

Digital Object Identifier 10.1109/ACCESS.2022.3168826

Ultra-Broadband RCS Reduction Based on Optimized Coding "Whale-Shaped" Polarization Conversion Metasurface With Angular Stability

ZHONGRU REN[1,2], YONG-QIANG LIU[2], YAN WANG[2], LAN LU[2], KAINAN QI[2], AND HONGCHENG YIN[1,2]

[1]School of Information and Communication Engineering, Communication University of China, Beijing 100024, China
[2]Science and Technology on Electromagnetic Scattering Laboratory, Beijing 100854, China

Corresponding authors: Yong-Qiang Liu (liuyq1990@126.com) and Hongcheng Yin (yinhc207@126.com)

ABSTRACT In this paper, we employed an efficient polarization conversion metasurface (PCM) to achieve broadband radar cross section (RCS) reduction for plane targets. Simulation results illustrate that the proposed "whale-shaped" unit achieves more than 90% polarization conversion ratio (PCR) in an ultra-broadband from 8.37 to 22.67 GHz. We combine the PCM unit into a 3 × 3 scale lattice to form periodic structure. Subsequently, we employ the PCM lattice and its mirror lattice as "Lattice 0" and "Lattice 1" of digital coding. In order to achieve the best RCS reduction performance, we obtain the optimized combinational layout by utilizing information entropy theory and genetic algorithm. Different from the traditional checkerboard distribution, the optimized coding PCM realizes scattering beam diffusion in space. The fitting of measurements and simulations demonstrate that the proposed PCM realizes monostatic RCS reduction of −10dB in the ultra-broadband from 9.37 to 22.79 GHz. Simultaneously, the proposed optimized coding PCM operates over a wide-angle oblique incidence range from 0° to 45°. The proposed "whale-shaped" optimized coding PCM features both ultra-broadband operating bandwidth and high angular stability, which is informative for the practical application for PCMs.

INDEX TERMS Polarization conversion metasurface, ultra-broadband, electromagnetic stealth, angular stability, polarization conversion ratio.

I. INTRODUCTION

The development of electromagnetic (EM) stealth technology is attached great importance by major military countries [1]. In order to improve the survivability of military weapons, it is imperative to promote the research on EM stealth technology. RCS is an important physical parameter to quantify the EM scattering ability of the targets, and the traditional RCS reduction methods mainly include surface shaping and radar absorbing materials coating [2]–[4]. However, for aircraft, the traditional method will sharply degrade its aerodynamic performance, and significantly increase the cost.

Different from traditional material-type EM absorbers, such as ferrite [5] and carbonyl iron [6], they directly absorb the incident EM energy through the material's loss characteristics. The research on metamaterials provides a feasible way to manipulate EM waves, such as EM cloak [7], metalens [8], planar retroreflector [9] and perfect EM absorber [10], etc. As the 2-D equivalent of metamaterials, researchers have achieved numerous works to reduce RCS using metasurfaces in recent years. For instance, Reference [11] employed two kinds of artificial magnetic conductor (AMC) units with 180° phase difference in broadband to form a checkerboard structure, which achieves monostatic RCS reduction of −10dB in the frequency range from 14.5 to 22 GHz. Metasurfaces can also absorb EM energy. For instance, the surface plasmon polariton (SPP) exhibits absorption characteristics near the cut-off frequency through its dispersion. Using this property, a low scattering antenna array based on SPP was proposed, which realizes monostatic RCS reduction in the frequency range from 6 to 14 GHz without affecting its radiation ability [12]. In addition to the above two stealth mechanisms, metasurfaces can also guide EM waves to propagate along the object surface. In reference [13], a smart Doppler cloak was fabricated by time-modulated reflective metasurface, which realizes EM stealth for moving targets.

The associate editor coordinating the review of this manuscript and approving it for publication was Wenjie Feng.

Polarization is an important characteristic of EM wave. Applications such as wireless communication, satellite positioning and radar tracking have special requirements for polarization characteristics. Traditional optical gratings or dichroic crystals [14], [15] can be utilized to change the polarization mode of the EM wave, but it has the disadvantages of large volume and low efficiency. Many published literatures have reported various types of PCM units [16]–[18]. However, the conversion efficiency and operating bandwidth of PCM units need to be improved. In recent years, researchers make remarkable progress in monostatic RCS reduction employing PMCs [19], [20], but extending the operating bandwidth and maintaining high angular stability is still a formidable challenge.

In order to realize the ultra-broadband monostatic RCS reduction, we proposed the "whale-shaped" PCM unit, which satisfies PCR exceeds 90% in the frequency range from 8.37 to 22.67 GHz. Simultaneously, in order to expand the scale of the unit cell, we combine 3 × 3 PCM units with the same size into a lattice to meet the periodic boundary conditions. PCM lattice and its mirror lattice are expressed as "Lattice 0" and "Lattice 1", respectively. The phase difference between the two lattices maintains at 180°±37° in the operating frequency band. We applied information entropy theory and global genetic algorithm to optimize the combinational layout [21]. Finally, through the reflection cancellation between the lattices, the reflected EM wave energy can be uniformly scattered in all directions. Optimized coding PCM still provides excellent manipulation of scattering field while the incident angle is increased. We manufactured the sample through PCB technique, and the experimental measurements illustrate that the sample realizes −10dB backward RCS reduction in the frequency range from 9.37 to 22.79 GHz. Moreover, when the oblique incidence angle reaches 45°, the sample still ensures the ultra-broadband RCS reduction effect.

II. UNIT DESIGN

In this work, a reflective linear cross-PCM unit composed of three-layer structure is proposed. The top layer is composed of a short line and two split oval rings of different sizes, and the shape of the pattern looks like a whale swimming in the vast ocean. The substrate layer is made of F4B-220, with a relative dielectric constant of $\varepsilon_r = 2.20$. The bottom layer is a continuous copper film. With the existence of the metal plane, reflective PCMs generally have higher PCR and larger operating bandwidth. Table 1 illustrates the geometric parameters of the unit cell. Due to the symmetric of the whole structure, it features polarization insensitive.

In order to quantify the conversion performance of the PCM, we defined several physical parameters. Assuming that the EM wave is incident normally along the -Z direction, the polarization mode of the electric field is x-polarized (TM- mode). Then, r_{xx} represents the co-polarized reflection coefficient, and r_{yx} represents the cross-polarized reflection coefficient [22]. Therefore, PCR can be expressed as

$$PCR = \frac{r_{yx}^2}{r_{yx}^2 + r_{xx}^2} \tag{1}$$

We employed full wave EM simulation software CST to calculate the characteristics of the proposed artificial structure. It is worth noting that the unit cell boundary condition is utilized for the x-y axes to approximate the infinite periodic structure [23], and the open add space boundary condition is utilized for the z-axis.

Fig. 2 shows that under the conditions of two polarization modes (TE mode & TM mode), the cross-polarized reflection coefficient of the PCM remains above −1dB in the frequency range from 8.37 to 22.67 GHz. Resonance occurs at the frequency points of 9.27 GHz, 13.81 GHz and 21.08 GHz, respectively. Fig. 3 shows the PCR of the whale-shaped PCM, which corresponds to the reflection coefficients and achieves more than 90% PCR in the operating frequency band from

TABLE 1. Geometric parameters of PCM unit.

Parameter	Value (mm)	Parameter	Value (mm)
P	5	H	3
L_1	6	W_1	0.3
R_1	2.4	W_2	0.2
R_2	1.6	W_3	0.25

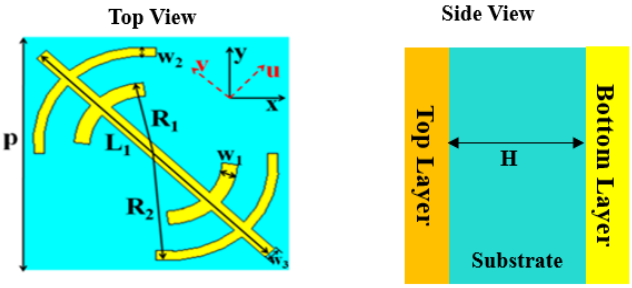

FIGURE 1. Schematic diagram of the proposed PCM unit.

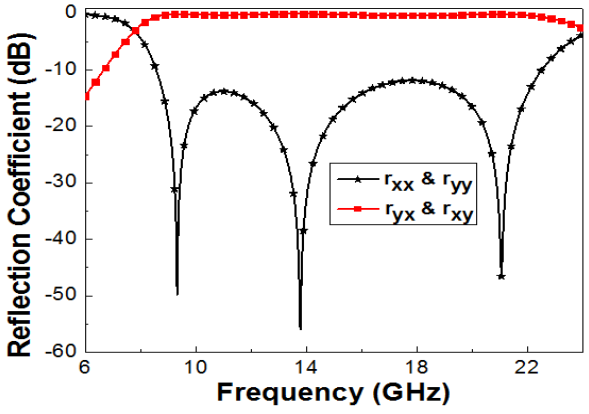

FIGURE 2. When the incident EM wave is in different polarization directions, co- and cross- polarized reflection coefficients.

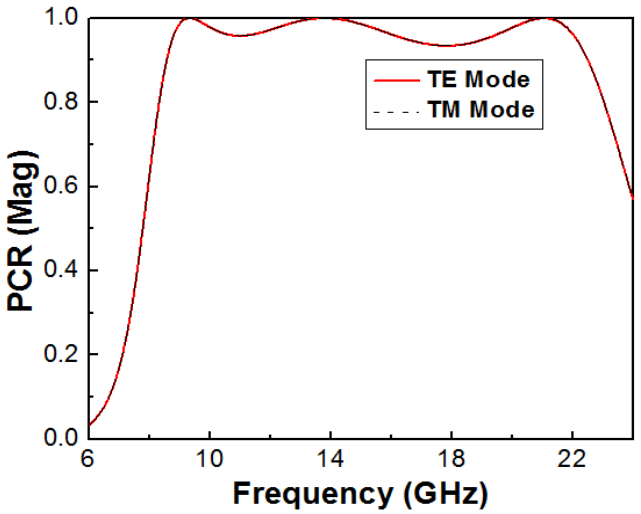

FIGURE 3. Simulated PCR of the proposed PCM in TE and TM mode.

8.37 to 22.67 GHz. The physical mechanism of the PCM unit can be analyzed by the equivalent circuit method, and many published works provide the specific procedure of fitting the RLC resonant circuit according to the EM resonance between the top and bottom layers [24]–[26]. The equivalent method is also applicable to the proposed "whale-shaped" structure.

III. PHYSICAL MECHANISM ANALYSIS

Rotating the x-y coordinate system 45° counterclockwise, then we will obtain the u-v coordinate system. If the direction of the incident electric field is along the u-axis or v-axis, different resonant modes will generate. According to the definition of EM polarization characteristics, the EM wave of any polarization mode can be decomposed into two orthogonal linear-polarized EM waves. Therefore, we can decompose the incident wave E_i and reflected wave E_r along the u-v coordinate system.

Fig. 4 reveals the relationship between the co-polarized reflectance and reflection phase of u-v axes. The incident

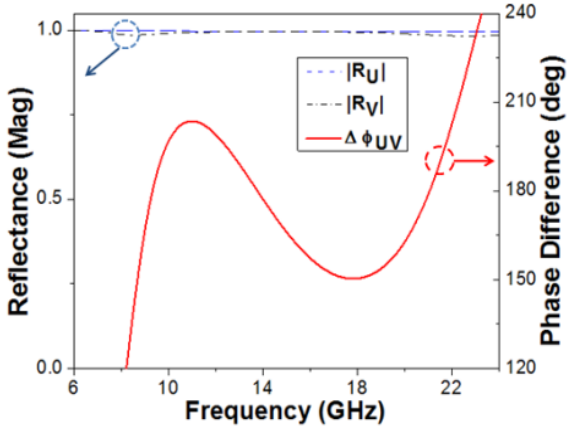

FIGURE 4. Co-polarized reflectance (R_u& R_v) and phase difference of the u-v coordinate system.

electric field and the reflected electric field are expressed as:

$$E_i = (E_{vi}\vec{e_v} + E_{ui}\vec{e_u}) \cdot \exp(jkz) \tag{2}$$

$$E_r = R \cdot E_i = (\vec{e_u}\ \vec{e_v}) \begin{pmatrix} |R_u| & 0 \\ 0 & |R_v| \end{pmatrix} \begin{pmatrix} E_{ui} \\ E_{vi} \end{pmatrix} \cdot \exp(-jkz - j\Delta\varphi_{uv}) \tag{3}$$

Owing to the symmetry of PCM unit about the u-v axes, when the incident wave is u-polarized or v-polarized, the reflected wave has no cross-polarized reflection coefficient. Under the condition of neglecting the loss, the bottom layer can reflect all the EM energy, which meets the amplitude requirements in Equation (3). Similarly, utilizing the 2-D anisotropy of the PCM, the u-v axes reflection phase difference in the operating frequency band maintains within 180±37° [27]. The electric field components in u and v directions can be synthesized. Finally, the polarization direction of the incident electric field converts to its orthogonal direction [28].

In order to explore the resonance mechanism of the whale-shaped PCM unit, we analyzed the surface current distribution of the unit at three resonance frequencies. If the incident EM wave is considered as an excitation signal, both the top layer and the bottom layer will emerge surface current. At resonance frequencies of 9.27 GHz and 13.81 GHz, the induced currents in the metal pattern and the bottom layer are in opposite directions, so the resonance characteristic is caused by magnetic resonance. Using the same analysis method, at the frequency of 21.08 GHz, the currents of the two layers are in the same direction, so the resonance characteristic is derived from electrical resonance.

IV. DESIGN OF THE "OPTIMIZED CODING PCM"

In the related applications of PCM so far, most of the works combine the PCM unit and its mirror unit into a simple checkerboard surface [29], and reduce the backward RCS of the target through the principle of reflection cancellation. This method does reduce the target's monostatic RCS, but increases the probability of being detected by enemy radars in other angular domains. In this work, based on the design idea of coding metasurface [30], [31], the units are formed into a 3 × 3 lattice, which enlarges the scale of the basic elements and weakens the mutual coupling between adjacent units.

Firstly, the number of "Lattice 0" and "Lattice 1" is determined. According to the design process of the coding metasurface, when the plane wave is incident normally, the scattering field E_S of the reflective metasurface is regarded as the superposition of all lattices. It can be expressed as:

$$\begin{aligned} E_s &= \sum_{a=1}^{A}\sum_{b=1}^{B} E_{ab}(\theta,\phi) \cdot e^{\psi_{ab}} \\ &= E_{ab}\sum_{a=1}^{A}\sum_{b=1}^{B} \exp\{j(a-0.5)(Dk\sin\theta\cos\phi) \\ &\quad + j(b-0.5)(Dk\sin\theta\sin\phi) + \psi_{ab}\} \end{aligned} \tag{4}$$

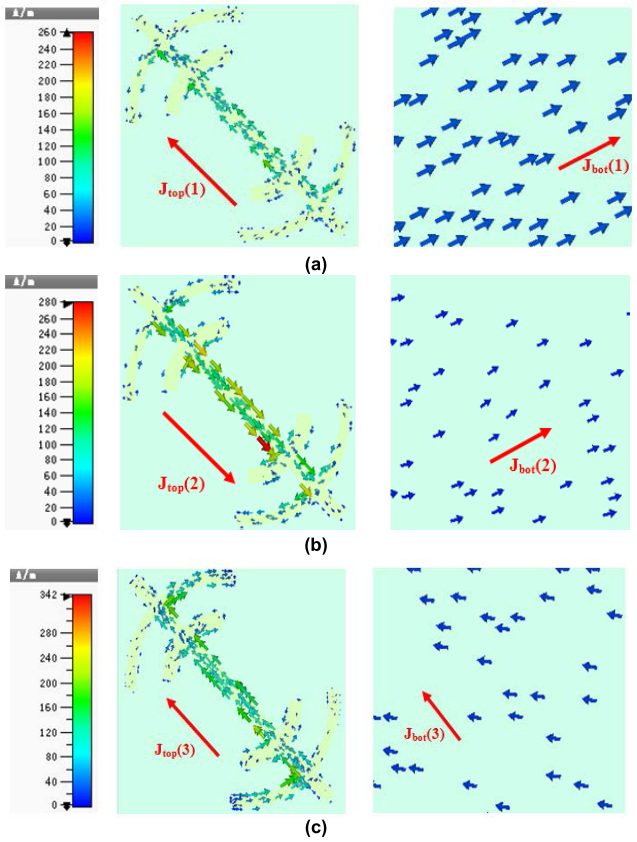

FIGURE 5. Surface distribution of the PCM unit. (a) @ 9.27 GHz, (b) @13.81 GHz, (c) @ 21.08 GHz.

where E_{ab} represents the scattered field function of each lattice, ψ_{ab} represents the reflection phase of each lattice, and D represents the period of the lattice. Since the reflection phase of each lattice can only be 0° or 180°, assuming that the probability of selecting each lattice is p, the discrete random variable F about the number of lattices obeys binomial distribution. Referring to the concept of information entropy in communications, we employ the information entropy H to present the smallest monostatic RCS in operating frequency band.

$$H = -p\log p - (1-p)\log(1-p) \tag{5}$$

Fig.6 shows the relationship between H and p. Obviously, when $p = 0.5$, the maximum value of information entropy H is 1. Besides, the number of "Lattice 0" and "Lattice 1" account for half of the total amount of basic elements.

With the number of lattices determined, the next issue is to determine the combinational layout quickly and accurately. Global genetic algorithm (GA) is undoubtedly the most suitable solution to this problem.

Since the final expected PCM size is 180mm × 180mm, the side length of each lattice is 15mm, the total number of lattice divisions is 144. According to formula (4), the reflection phase of each lattice can be superimposed to obtain the total scattering field of the optimized coding PCM.

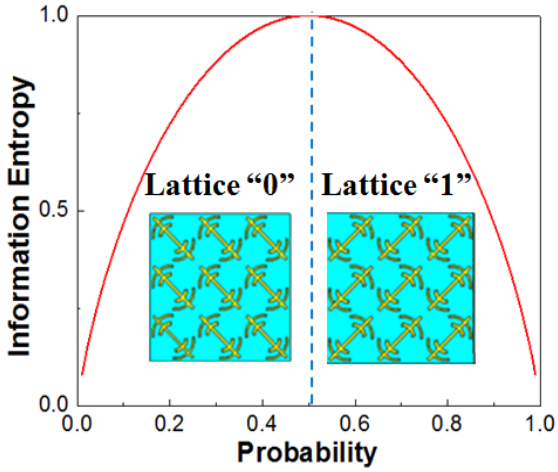

FIGURE 6. Functional relationship between H &p.

Therefore, we use A^* to represent the reflection phase of each lattice, which is equivalent to the variable matrix. However, as depicted in Fig. 7 (a), after setting the fitness function as *max(Es)*, GA outputs the minimum fitness function value and the corresponding variable matrix A^* through five processes: population initialization, fitness calculation, selection, crossover and mutation.

This design utilizes the idea of coding metamaterial for reference, reasonably combines multiple 0-1 lattices, and then enhances the interference cancellation between adjacent lattices. Finally, it affects the distribution of the scattering field and reduces the RCS of each angular domain of the plane target. In order to verify the effect of the proposed optimization method on the RCS reduction, we compared the performance of the optimized coding PCM and the uniform coding PCM with the same size. It is worth mentioning that the so-called uniform coding PCM arranges the 0-1 lattice in a cross distribution manner. It can be seen from the 3-D far-field scattering diagram in Fig. 8(a) that the uniform coding PCM has only two abnormal reflected directions. Comparing with the PEC plane, it does reduce a small part of the monostatic RCS, but the EM energy in abnormal reflected directions is enhanced. By contrary, the optimized coding PCM can evenly diffuse the incident EM energy to each angular domain in space. Simulation results prove that we have achieved scattering beam diffusion. Fig. 8(b) illustrates that the backward RCS reduction of −10dB is achieved in the ultra-broadband from 9.52 to 23.24 GHz.

In practical engineering applications, not all the EM energy will be incident on the PCM normally. Therefore, "optimized coding PCM" is required to ensure stable RCS reduction capability under the condition of oblique incidence. Fig. 9 shows the reduction of backward RCS when the EM wave is incident obliquely from 0° to 45°. When the oblique incidence angle reaches 45°, the EM coupling effect between the top and bottom layers is weakened, so the bandwidth of backward RCS reduction is slightly narrowed. Simulation

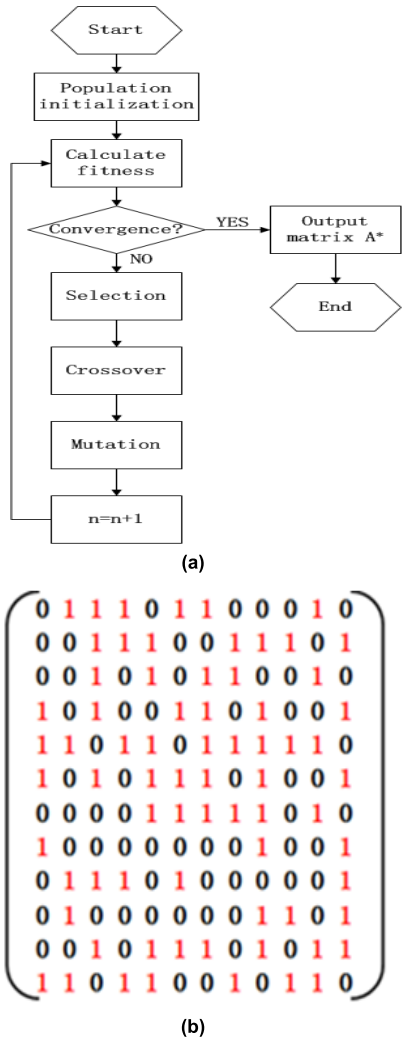

FIGURE 7. Optimization of lattice distribution by GA: (a) Program flow chart. (b) Lattice sequence matrix A*.

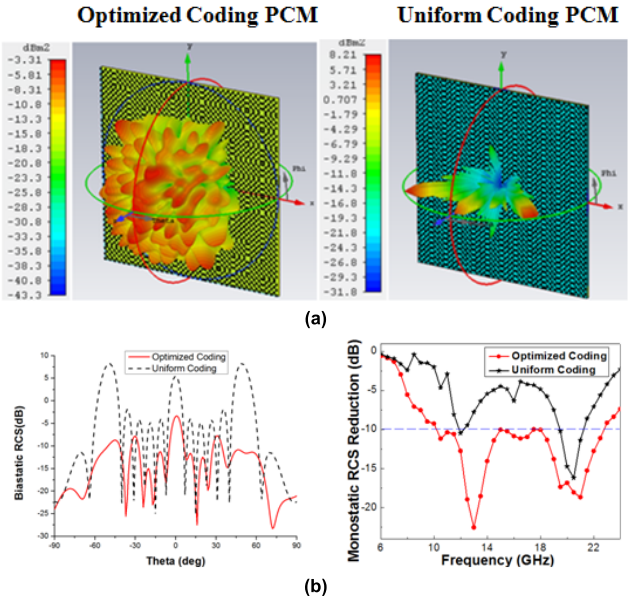

FIGURE 8. Comparison of the RCS reduction performance. (a) 3-D far-field scattering patterns, (b) Biastatic RCS when azimuth angle is 0° & broadband backward RCS reduction performance.

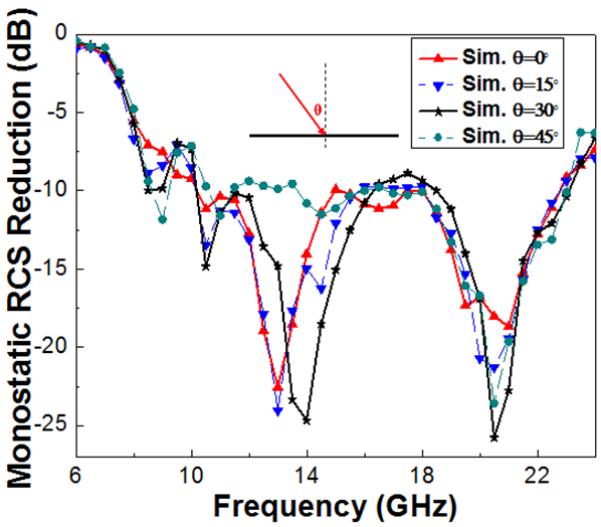

FIGURE 9. Simulated RCS reduction under oblique incidence (TM mode).

results demonstrate that the optimized coding PCM features high angular stability.

V. EXPERIMENTAL TESTS AND VERIFICATIONS

In order to verify the accuracy of the simulation results, the sample of the proposed "GA optimized coding PCM" was processed by PCB technique, and its geometric size is 180mm × 180mm. We built the required testing system in the microwave anechoic chamber. After preheating and calibration, two broadband horn antennas for transmitting and receiving signals are connected to the vector network analyzer *Rohde & Schwarz-ZVA40*. We adjusted the center of the two antennas and the sample to the same height. In order to ensure that the plane wave is incident on the sample, the horizonal distance between the antennas and the sample needs to meet the far-field conditions $D > 2L^2/\lambda$, where L represents the maximum aperture of the sample and λ represents the wavelength of the incident EM wave.

We measured the far-field reflection of the sample and the metal plane with the same size by free space method, and then the two measurement results are subtracted to obtain the RCS reduction of the sample relative to the metal plane. In the measurement process, signal-processing techniques such as background vector subtraction and time gate were used, which effectively reduce the background noise and measurement errors. The good fitness between the experimental measurements and the numerical simulations demonstrate that the sample does reduce the backward RCS of the planar target in ultra-broadband under normal incidence conditions. Experimental measurements demonstrate

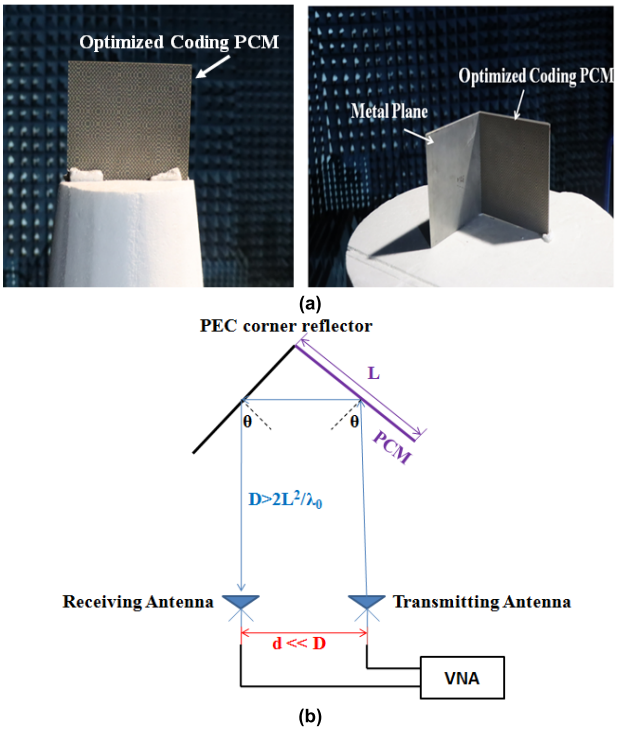

FIGURE 10. Experimental test of monostatic RCS: (a) Measurement environment of normal incidence and oblique incidence, (b) schematic diagram of measurement process.

that the operating bandwidth of −10dB RCS reduction is 9.37 to 22.79 GHz.

We noticed that many previous works have not carried out practical experiments on the obliquely incident RCS reduction. For the industrial production, it is not rigorous. As shown in Fig. 10, we utilized a metal sphere and a corner reflector for calibration, and then fixed the sample to one side of the corner reflector. Incident azimuth $\theta = 0°$ corresponding to the sample was facing the antenna. During the experiment, the horn antenna did not move, and then we rotated the corner reflector on the rotary table. Using this testing method, the monostatic RCS of the sample can be measured quickly and accurately. Finally, according to the testing method, we obtained the RCS reduction bandwidth measurements for incident azimuths of 15°, 30° and 45°, respectively. We found that the backward RCS reduction performance in the measurements was different from the expected simulation results, especially when $\theta = 15°$. We analyzed the causes of the errors: firstly, measurement errors, such as limited sample size or misalignment of the antennas with the sample. Secondly, the sample induces higher order mode under oblique incidence excitation.

In practical engineering, there are special requirements for low RCS metasurfaces under different application backgrounds. As mentioned in the introduction, many works involved RCS reduction methods, but they employed different unit types and array distribution. Two conclusions can be drawn from Table 2: Firstly, most applications of wideband RCS reduction basically utilize PGMs or AMCs.

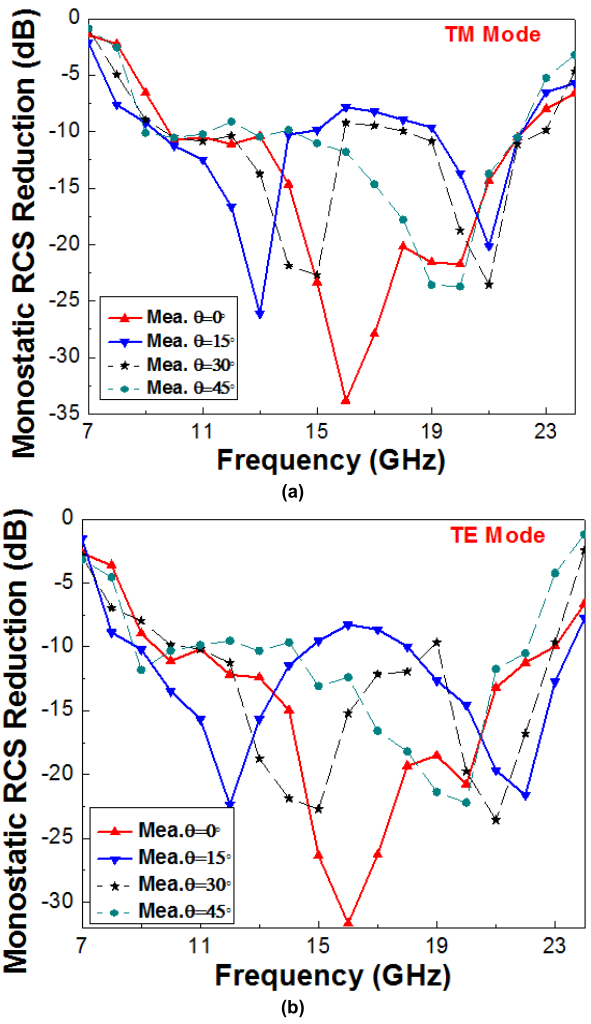

FIGURE 11. Measurements of RCS reduction: (a) TM mode, (b) TE mode.

TABLE 2. Comparison of performance with other structures.

Ref.	Unit Type	Array Distribution	O.B. (GHz)	F.BW. (%)	H/λ_L
[24]	AMC	GA optimized coding	5.4-7.4	31.3	0.05
[25]	AMC	Checkerboard	7.98-16.32	68.6	0.08
[26]	PGM	GA optimized coding	16.5-34.6	70.8	0.08
[27]	PCM	Checkerboard	5.7-7.7	29.8	0.08
[28]	AMC	Paticle swarm coding	15-35	80	0.11
This work	**PCM**	**GA optimized coding**	**9.37-22.79**	**83.5**	**0.08**

AMC: Artificial Magnetic Conductor. **PGM:** Phase Gradient Metasurface.
O. B.: Operating frequency band when backward RCS reduction of -10dB.
F. BW. : Fractional bandwidth.**H:** Actual thickness.
λ_L: Wavelength corresponding to the lowest frequency.

For the actual engineering needs of PCMs, it still needs to be explored [37]–[40]. Secondly, most PCM applications use traditional checkerboard layout. Secondly, the proposed

"optimized coding PCM" not only has an ultra-broadband operating bandwidth, but also features high angular stability.

VI. CONCLUSION

This article proposed a "whale-shaped" PCM unit with polarization insensitivity, low profile, and ultra-broadband operating bandwidth. Using the design process of coding metamaterials, we determined the number of different lattices through information entropy. Afterwards, the combinational layout was optimized by genetic algorithm. Finally, we measured the backward RCS reduction of the sample under normal and oblique incident conditions. The good fitting between simulations and measurements proves that the proposed optimized coding PCM achieves both ultra-broadband RCS reduction and angular stability. This work is instructive for addressing the challenge of balancing operation bandwidth and angular sensitivity.

REFERENCES

[1] E. F. Knott, J. F. Schaeffer, and M. T. Tulley, *Radar Cross Section*. Raleigh, NC, USA: SciTech, 2004.

[2] K. J. Vinoy, and R. M. Jha, *Radar Absorbing Materials: From Theory to Design and Characterization*. Norwell, MA, USA: Kluwer, 1996.

[3] B. Zhang and Z. Shen, "Wideband radar absorbing material combining high-impedance transmission line and circuit analogue screen," *Electron. Lett.*, vol. 44, no. 4, pp. 318–319, Feb. 2008.

[4] W. Jiang, Y. Liu, S. Gong, and T. Hong, "Application of bionics in antenna radar cross section reduction," *IEEE Antennas Wireless Propag. Lett.*, vol. 8, pp. 1275–1278, Nov. 2009.

[5] J. Y. Shin and J. H. Oh, "The microwave absorbing phenomena of ferrite microwave absorbers," *IEEE Trans. Magn.*, vol. 29, no. 6, pp. 3437–3439, Nov. 1993.

[6] Y. Feng, T. Qiu, C. Shen, and X. Li, "Electromagnetic and absorption properties of carbonyl iron/rubber radar absorbing materials," *IEEE Trans. Magn.*, vol. 42, no. 3, pp. 363–368, Mar. 2006.

[7] D. Schurig *et al.*, "Metamaterial elctromagnetic cloak at microwave frequencies," *Science*, vol. 314, no. 5801, pp. 977–980, Nov. 2006.

[8] Y. Liu *et al.*, "Broadband, large-numerical-aperture and high-efficiency microwave metalens by using a double-layer transmissive metasurface," *Appl. Phys. Exp.*, vol. 15, no. 1, Jan. 2022, Art. no. 014003.

[9] Y. Liu, S. Li, J. Guo, L. Li, and H. Yin, "Planar microwave retroreflector based on transmissive gradient index metasurface," *New J. Phys.*, vol. 22, no. 6, Jun. 2020, Art. no. 063044.

[10] N. I. Landy, S. Sajuyigbe, J. J. Mock, D. R. Smith, and W. J. Padilla, "Perfect metamaterial absorber," *Phys. Rev. Lett.*, vol. 100, no. 20, May 2008, Art. no. 207402.

[11] J. C. I. Galarregui, A. T. Pereda, J. L. M. de Falcon, I. Ederra, R. Gonzalo, and P. de Maagt, "Broadband radar cross section reduction using AMC technology," *IEEE Trans. Antennas. Propag.*, vol. 61, no. 12, pp. 6136–6143, Dec. 2013.

[12] Y. Han, J. Wang, S. Gong, Y. Li, Y. Zhang, and J. Zhang, "Low RCS antennas based on dispersion engineering of spoof surface plasmon polaritons," *IEEE Trans. Antennas. Propag.*, vol. 66, no. 12, pp. 7111–7116, Dec. 2018.

[13] X. Zhang *et al.*, "Smart Doppler cloak operating in broadband and full polarizations," *Adv. Mater.*, vol. 33, no. 17, Apr. 2021, Art. no. 2007966.

[14] D. Broer, J. Lub, and G. Mol, "Wide-band reflective polarizers from cholesteric polymer networks with a pitch gradient," *Nature*, vol. 378, pp. 467–479, Nov. 1995.

[15] F. Robert, P. Besnard, M. L. Chares, and G. M. Stephan, "Polarization modulation dynamics of vertical-cavity surface-emitting lasers with an extended cavity," *IEEE J. Quantum Elect.*, vol. 33, no. 12, pp. 2231–2239, Dec. 1997.

[16] B. Lin, L. Lv, J. Guo, Z. Liu, X. Ji, and J. Wu, "An ultra-wideband reflective linear-to-circular polarization converter based on anisotropic metasurface," *IEEE Access*, vol. 8, pp. 82732–82740, Apr. 2020.

[17] J. Xu, R. Li, J. Qin, S. Wang, and T. Han, "Ultra-broadband wide-angle linear polarization converter based on H-shaped metasurface," *Opt. Exp.*, vol. 26, no. 16, Aug. 2018, Art. no. 20913.

[18] M. Karamirad, C. Ghobadi, and J. Nourinia, "Metasurfaces for wideband and efficient polarization rotation," *IEEE Trans. Antennas. Propag.*, vol. 69, no. 3, pp. 1799–1804, Mar. 2021.

[19] T. Hong, S. Wang, Z. Liu, and S. Gong, "RCS reduction and gain enhancement for the circularly polarized array by polarization conversion metasurface coating," *IEEE IEEE Antennas Wireless Propag. Lett.*, vol. 18, no. 1, pp. 167–171, Jan. 2019.

[20] Q. Zheng, C. Guo, G. A. E. Vandenbosch, and J. Ding, "Low-profile circularly polarized array with gain enhancement and RCS reduction using polarization conversion EBG structures," *IEEE Trans. Antennas. Propag.*, vol. 68, no. 3, pp. 2440–2445, Mar. 2020.

[21] S. Li *et al.*, "Ultra-broadband reflective metamaterial with RCS reduction based on polarization convertor, information entropy theory and genetic optimization algorithm," *Sci. Rep.*, vol. 6, Nov. 2016, Art. no. 37409.

[22] H. Sun *et al.*, "Broadband and broad-angle polarization-independent metasurface for radar cross section reduction," *Sci. Rep.*, vol. 7, no. 1, Feb. 2017, Art. no. 407821.

[23] B. Lin *et al.*, "Ultra-wideband and high-efficiency reflective polarization converter for both linear and circular polarized waves," *Appl. Phys. A, Solids Surf.*, vol. 125, no. 2, p. 76, Jan. 2019.

[24] C. Ni, M. S. Chen, Z. X. Zhang, and X. L. Wu, "Design of frequency-and polarization-reconfigurable antenna based on the polarization conversion metasurface," *IEEE IEEE Antennas Wireless Propag. Lett.*, vol. 17, no. 1, pp. 78–81, Jan. 2018.

[25] P. Xie, G. Wang, H. Li, J. Liang, and X. Gao, "Circularly polarized fabry-perot antenna employing a receiver-transmitter polarization conversion metasurface," *IEEE Trans. Antennas. Propag.*, vol. 68, no. 4, pp. 3213–3218, Apr. 2020.

[26] J. Wang, R. Yang, R. Ma, J. Tian, and W. Zhang, "Reconfigurable multifunctional metasurface for broadband polarization conversion and perfect absorption," *IEEE Access*, vol. 8, pp. 105815–105823, Jun. 2020.

[27] H. Li, L. Yuan, B. Zhou, X. Shen, Q. Cheng, and T. Cui, "Ultrathin multiband gigahertz metamaterial absorbers," *J. Appl. Phys.*, vol. 110, no. 1, Jul. 2011, Art. no. 014909.

[28] X. Yang, Z. Ding, and Z. Zhang, "Broadband linear polarization conversion across complete Ku band based on ultrathin metasurface," *Int. J. Electron. Commun.*, vol. 139, Jul. 2021, Art. no. 153884.

[29] J. D. Baena, S. B. Glybovski, J. P. del Risco, A. P. Slobozhanyuk, and P. A. Belov, "Broadband and thin linear-to-circular polarizers based on self-complementary zigzag metasurfaces," *IEEE Trans. Antennas Propag.*, vol. 65, no. 8, pp. 4124–4133, Aug. 2017.

[30] T. Cui, M. Qi, X. Wan, J. Zhao, and Q. Cheng, "Coding metamaterials, digital metamaterials and programmable metamaterials," *Light, Sci. Appl.*, vol. 3, no. 10, p. e218, Oct. 2014.

[31] S. Liu and T. J. Cui, "Flexible controls of terahertz waves using coding and programmable metasurfaces," *IEEE J. Sel. Topics Quantum Electron.*, vol. 23, no. 4, pp. 1–12, Aug. 2017.

[32] X. Liu, J. Gao, L. Xu, X. Cao, Y. Zhao, and S. Li, "A coding diffuse metasurface for RCS reduction," *IEEE Antennas Wireless Propag. Lett.*, vol. 16, pp. 724–727, Apr. 2017.

[33] S. H. Kim and Y. J. Yoon, "Wideband radar cross-section reduction on checkerboard metasurfaces with surface wave suppression," *IEEE Antennas Wireless Propag. Lett.*, vol. 18, no. 5, pp. 896–900, May 2019.

[34] S. Koziel, M. Abdullah, and S. Szczepanski, "Design of high-performance scattering metasurface through optimization-based explicit RCS reduction," *IEEE Access*, vol. 9, pp. 113077–113088, Aug. 2021.

[35] W. Zhang, Y. Liu, and Y. Jia, "Circularly polarized antenna array with low RCS using metasurface-inspired antenna units," *IEEE Antennas Wireless Propag. Lett.*, vol. 18, no. 7, pp. 1453–1457, Jul. 2019.

[36] H. Hao, S. Du, and T. Zhang, "Small-size broadband coding metasurface for RCS reduction based on particle swarm optimization algorithm," *Prog. Electromagn. Res. M*, vol. 81, pp. 97–105, Jan. 2019.

[37] Y. Ran, J. Liang, T. Cai, and H. Li, "High-performance broadband vortex beam generator using reflective Pancharatnam-Berry metasurface," *Opt. Commun.*, vol. 427, pp. 101–106, Nov. 2018.

[38] Y. Fu, Y. Li, and N. Yuan, "Wideband composite AMC surfaces for RCS reduction," *Microw. Opt. Technol. Lett.*, vol. 53, no. 4, pp. 712–715, Apr. 2011.

[39] J. Su, Y. Lu, J. Liu, Y. Yang, Z. Li, and J. Song, "A novel checkerboard metasurface based on optimized multielement phase cancellation for super-wideband RCS reduction," *IEEE Trans. Antennas Propag.*, vol. 66, no. 12, pp. 7091–7099, Dec. 2018.

[40] C. Vasanelli, F. Bögelsack, and C. Waldschmidt, "Reducing the radar cross section of microstrip arrays using AMC structures for the vehicle integration of automotive radars," *IEEE Trans. Antennas Propag.*, vol. 66, no. 3, pp. 1456–1464, Mar. 2018.

ZHONGRU REN was born in Jilin, China, in 1996. He received the master's degree in physics and electronics from the Communication University of China, Beijing, China, in 2020, where he is currently pursuing the Ph.D. degree in electromagnetic fields and microwave techniques.

He worked as an Assistant Engineer with the Science and Technology on Electromagnetic Scattering Laboratory, Beijing, in 2021. At present, he has published several IEEE and EI retrieval papers. His research interests include polarization conversion metasurfaces, modeling of complex electromagnetic scattering targets, metasurface-based RCS reduction, and radiation-scattering integrated antennas.

YONG-QIANG LIU was born in Sichuan, China, in 1990. He received the B.S. degree from the College of Electronic Science and Engineering, Jilin University, Changchun, China, in 2012, and the Ph.D. degree from the School of Electronics Engineering and Computer Science, Peking University, Beijing, China, in 2017.

He is currently a Senior Engineer with the Science and Technology on Electromagnetic Scattering Laboratory, Beijing. He has authored or coauthored over 30 peer-reviewed journals and conference papers. His current research interests include plasmonics, metamaterials and related microwave, and millimeter wave-THz functional devices.

YAN WANG was born in Heilongjiang, China, in 1988. She received the master's degree in aeronautical engineering from the Beijing University of Aeronautics and Astronautics, Beijing, China, in 2013. She is currently a Researcher with the Science and Technology on Electromagnetic Scattering Laboratory, Beijing Institute of Environmental Features. She has published many articles in some important academic journals. Her research interests include electromagnetic scattering test technology and radar absorbing structure.

LAN LU was born in Gansu, China, in 1994. He received the Graduate degree from the Nanjing University of Aeronautics and Astronautics, Nanjing, China. He is currently working with the the Science and Technology on Electromagnetic Scattering Laboratory, Beijing Institute of Environmental Features. His research interests include electromagnetic scattering, metamaterials, and frequency selective surface.

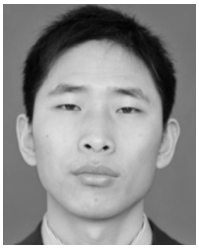

KAINAN QI was born in Shandong, China, in 1986. He received the B.S. degree in electronic information engineering from Xi'dian University, Xi'an, China, in 2008, and the Ph.D. degree in electromagnetic field and microwave technology from the Communication University of China, Beijing, China, in 2021.

Since 2017, he has been a Senior Engineer with the Science and Technology on Electromagnetic Scattering Laboratory. His current research interests include the frequency selective surface and reconfigurable metasurface.

HONGCHENG YIN was born in Jiangxi, China, in 1967. He received the Ph.D. degree in electromagnetic field and microwave technique from Southeast University, Nanjing, China, in 1993.

He is currently a Research Fellow with the Science and Technology on Electromagnetic Scattering Laboratory, Beijing Institute of Environmental Features. He has coauthored four books and published more than 130 articles in domestic and foreign academic journals. His research interests include electromagnetic scattering and inverse scattering, radar target characteristics, and radar target recognition. He is a fellow of the Chinese Institute of Electronics.